Nano Research
2020, 13(1): 183–187

ISSN 1998-0124 CN 11-5974/O4
https://doi.org/10.1007/s12274-019-2593-3

Research Article

In situ observation of temperature-dependent atomistic and mesoscale oxidation mechanisms of aluminum nanoparticles

Jing Gao, Jingyuan Yan, Beikai Zhao, Ze Zhang, and Qian Yu (✉)

Center of Electron Microscopy and State Key Laboratory of Silicon Materials, School of Materials Science and Engineering, Zhejiang University, Hangzhou 310027, China

Received: 18 August 2019 / **Revised:** 6 November 2019 / **Accepted:** 2 December 2019

ABSTRACT

Oxidation is a universal process causing metals' corrosion and degradation. While intensive researches have been conducted for decades, the detailed atomistic and mesoscale mechanisms of metal oxidation are still not well understood. Here using *in situ* environmental transmission electron microscopy (E-TEM) with atomic resolution, we revealed systematically the oxidation mechanisms of aluminum from ambient temperature to ~ 600 °C. It was found that an amorphous oxide layer formed readily once Al was exposed to air at room temperature. At ~ 150 °C, triangle-shaped Al_2O_3 lamellas grew selectively on gas/solid (oxygen/amorphous oxide layer) interface, however, the thickness of the oxide layer slowly increased mainly due to the inward diffusion of oxygen. As the temperature further increased, partial amorphous-to-crystallization transition was observed on the amorphous oxide film, resulting in the formation of highly dense nano-cracks in the oxide layer. At ~ 600 °C, fast oxidation process was observed. Lamellas grew into terraces on the oxide/gas interface, indicating that the high temperature oxidation is controlled by the outward diffusion of Al. Single or double/multi-layers of oxide nucleated at the corners of the terraces, forming dense γ'-Al_2O_3, which is a metastable oxide structure but may be stabilized at nanoscale.

KEYWORDS

in situ transmission electron microscopy (TEM), aluminum oxidation, temperature, diffusion

1 Introduction

Aluminum (Al) is one of the most important light-weight structural metals utilized in industry, as well as one showing substantial activeness of being oxidized in aerobic environment. The oxidation processes of Al have been extensively studied for decades and different oxidation mechanisms were put forward based on the widely recognized Cabrera-Mott oxidation theory [1–7]. Generally, oxidation begins with chemisorption of oxygen on the metal surface and then oxygen interacts with metal atoms to form a thin oxide layer. The further thickening process at low temperatures is advanced by the two-way transportation of oxygen and metal ions across the oxide film, which is driven by the strong electric field (often called Mott filed) introduced by the difference of contact potentials between metal and adsorbed oxygen. The surface-charge field weakens with the thickening of the oxide film and as a result, the formed oxide films exist upper limits of thickness. The metal-oxygen reaction is sensitive to temperature. A slight rise not only directly enhances the diffusion coefficient of ions, but also produces the inhomogeneous stress, caused by the difference of thermal expansion coefficient between metal and oxide film, which also promotes the outward diffusion of metal ions.

Aluminum nanoparticles, with considerable reactivity and enthalpy of combustion, are widely applied in propellants to amplify the energy released during the reaction and thus enhance the reaction temperature [8]. A. Dokhan et al. found that particle size had a significant impact on the reaction performance; adding ultra-fine aluminum particles in ammonium perchlorate (AP) solid propellants could increase the burning rate. Owing to the high reactivity of aluminum with surrounding oxygen [9–11], aluminum nanoparticles are usually coated with a thin alumina film with thickness of 2 to 4 nm even at low temperatures [12], which results in a much higher oxide volume fraction than that of its bulk counterpart. Based on this, the alumina films in nanoparticles play special and significant roles in fields such as microelectronics, catalysis, metal protection and anti-corrosion applications. There have been extensive efforts on studying the oxidation process and mechanism of aluminum nanoparticles [13–19], numerous of which show that oxidation process of aluminum powders roughly goes through four stages as temperature increases from room temperature to ~ 1,500 °C: amorphous phase, γ-Al_2O_3, transient phase θ-Al_2O_3, and stable α-Al_2O_3 phase. The reaction rates of each stage vary since the ion diffusion rates change along with temperature. While phase transition is universally observed, the exact transition temperature is still under debate. Furthermore, the specific details of the oxidation process under different temperatures are not available hitherto. Here we performed the *in situ* transmission electron microscopy (TEM) investigation on Al nanoparticle in oxygen atmosphere from room temperature to ~ 600 °C, in order to study the dynamic oxidation process and the corresponding mechanisms.

Address correspondence to yu_qian@zju.edu.cn

2 Experimental

2.1 Sample preparation

Single crystal aluminum nanoparticles were produced by a direct current (DC) arc plasma method, as reported previously [16]. The particles used for our *in situ* test were ~ 40 nm in diameter. We prepared the samples by suspending the Al nanoparticles in ethanol in a test tube and separating the individual particles by ultrasonic vibration for 7,200 s.

2.2 Experimental procedure

The atomic structure of Al/Al_2O_3 as well as the energy dispersive X-ray spectroscopy (EDX) map was obtained by using an aberration corrected Titan G2 80-200kV/ChemiSTEM operated at 200 kV at room temperature.

In situ oxidation experiments were performed in an environmental TEM (E-TEM) (Hitachi 9500) at 200 kV with oxygen injection available. An AMT digital camera and a DE-12 camera system (Direct Electron, LP) were employed to *in situ* record the dynamic reconstruction behaviors. The frame rates were set for 6 and 10 fps on AMT digital camera and DE-12 camera, respectively [20]. We controlled the O_2 pressure at ~ 8×10^{-2} Pa and the temperature ranging from room temperature to 600 °C. Low electron beam current as used in the previous article was applied in order to eliminate the effect of electron beam [21]. Firstly, we heated the sample to ~ 150 °C and held for over an hour. We increased the temperature by 10 °C every 5 min along with the observation of the oxidation process. When the temperature reached ~ 350 °C, the oxidation rate was fast and amorphous-to-crystallization transition occurred. We stayed at this temperature for about an hour till the phenomena hardly changed. The temperature was further increased to ~ 600 °C in a similar way. Another test was carried out on a Al nanoparticle which had been already heated at ~ 350 °C in the same condition as above. We continued to heat it up to ~ 400 °C and turned off the oxygen gas in order to study the formed nano-cracks on the oxide film.

3 Results and discussion

Figure 1(a) shows the typical morphology of a spherical aluminum nanoparticle with a relatively rough surface. As indicated by the fast Fourier transform (FFT) patterns in Fig. 1(b), an initial amorphous oxide layer (~ 3 nm in thickness) is around the aluminum core, which is consistent with the previous report [9]. The initial formation of the oxide film is usually amorphous rather than crystalline since the lattice mismatch between a crystalline substrate and epitaxial oxide generates intrinsic stress. Furthermore, amorphous oxides with a large fraction of free volume are skilled in relaxation of stress at relatively low temperature [22, 23]. Figure 1(b) shows a typical high angle annular dark field scanning transmission electron microscopy (HAADF-STEM) image, displaying the atomic structure of the interface between single crystal aluminum core and the shell of amorphous Al_2O_3. The arrangement of Al near the interface is essentially uniform with that in the core, which indicates the lattice distortion near the interface is negligible and the interfacial defect density could be considered quite low. In relatively larger particles, the thickness of the initial oxide layer is close to that shown in the EDX maps in Fig. 1(c).

The high resolution TEM images in Fig. 2 show the dynamic oxidation process from ambient temperature to ~ 400 °C. Temperature at ~ 150 °C was held for more than one hour, during which oxidation happened but was quite slow. Al_2O_3 lamellas, generally in triangle shape, appeared and grew selectively on the gas/solid interface as marked by the black arrows in Fig. 2. This is similar to the *in situ* oxidation results of the single crystal Mg nanoparticles by E-TEM at 130 °C [21]. As the temperature increased to ~ 350 °C (Fig. 2(b)), the thickness of the amorphous oxide layer increased by more than 1 nm. The interface between Al core and oxide film moved inward due to the inward chemical diffusion of oxygen. No apparent voids were formed at the aluminum/aluminum oxide interface. One-dimensional lattice fringes appeared locally in the amorphous oxide film as marked by orange arrows in Fig. 2(b), indicating the amorphous oxide film started to crystallize heterogeneously. It was reported that intrinsic stress can be generated in amorphous Al_2O_3 films by thermal oxidation at room temperatures, which is related to the orientations of the aluminum substrate: Oxide films formed on Al(100) are stress free, whereas oxide films formed on Al(111) exhibit a thickness averaged in-plane tensile film stress as large as 1.9 GPa [23, 24]. According to this, we inferred that the inhomogeneous stress introduced

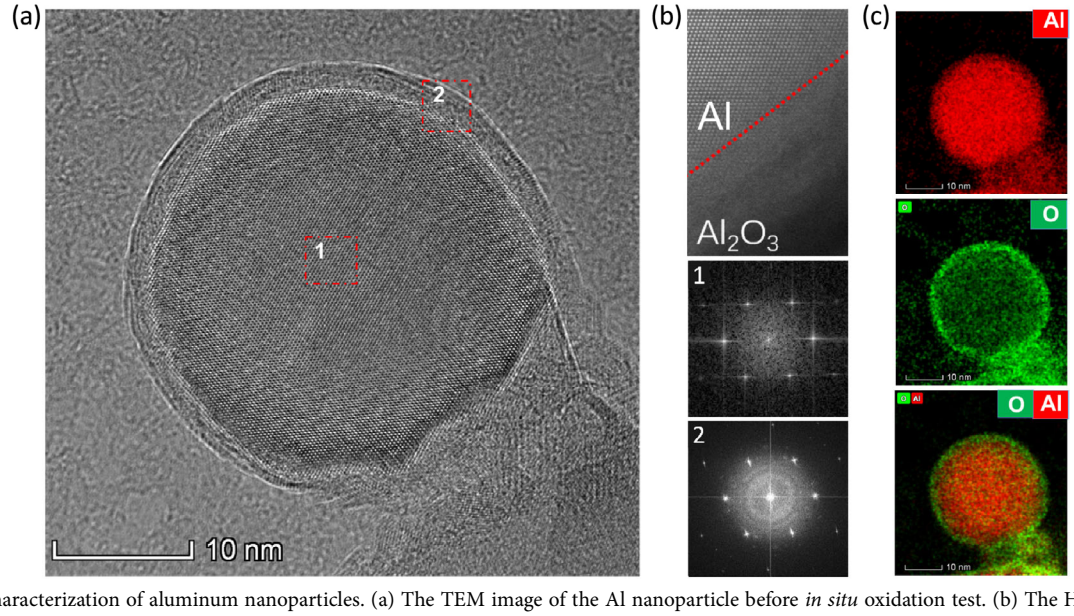

Figure 1 Characterization of aluminum nanoparticles. (a) The TEM image of the Al nanoparticle before *in situ* oxidation test. (b) The HAADF-STEM image of Al/Al_2O_3 interface. The corresponding FFT patterns of the material within the red dotted boxes marked in (a) demonstrate that the oxide layer is amorphous structure. (c) EDX maps of Al nanoparticle before test.

by the disparate orientation of Al induced the selective growth of lamellas and partial crystallization of amorphous materials [19, 25]. The crystalline temperature in our test is ultimately identical to the previous reports of L. P. H. Jeurgens et al. [26, 27].

To analyze the change of thickness of the oxide film at different oxidation stages, we plotted the contours of the gas/solid and solid/solid interface in Figs. 2(a) and 2(b), then spliced them together into Fig. 2(c) to show the evolution of the interface migration. The migration of the solid/solid interface was faster than that of the gas/solid interface, indicating that the inward diffusion of oxygen was the major controller of oxidation at 150–350 °C. With the thickening of the oxide film, effects of the Mott filed were gradually weakened by the constraint of coupled currents of electrons and cations, thus the oxidation rate gradually slowed down. As the temperature increased, Al diffusion rate was accelerated by the thermal expansion [13]. The solid/solid interface migrated further inward at 350 °C than at 150 °C especially near the crystallized oxide, which might be attributed to the elevated diffusion rate of oxygen along the grain boundaries caused by the crystalline of the amorphous oxide film [18]. The two-way migration of gas/solid interface and solid/solid interface resulted in an increase of more than 1 nm in the thickness of the oxide film.

Afterwards we quickly increased the temperature to ~ 400 °C while keeping the O_2 pressure constant. Figure 2(d) shows a high resolution TEM image of a particle which had been at ~ 400 °C for 10 min. A large number of oxide lamellas distribute much more uniformly than that in Fig. 2(b).

Because crystal Al_2O_3 has higher density than amorphous phase, the intrinsic stress in the oxide film raised, resulting in the formation of cracks [23]. These cracks were quickly repaired by the newly formed oxide under oxygen atmosphere [13]. Since the TEM images only display a two-dimensional projection of the real three-dimensional objects, it is difficult to directly view the cracks. In order to investigate the distribution and density of cracks generated during the transition, we turned off the oxygen gas and merely heated the sample. It was speculated that aluminum would outward diffuse and the cracks might be identified since they served as the tunnels for aluminum diffusion [13, 28]. Figure 3 shows the typical dynamic process of producing the "popcorn"-shape aluminum nanoparticle by directly heating a nanoparticle that was previously oxidized at ~ 400 °C. It was observed that the outward diffusion of aluminum happened ubiquitously around the particle. It indicates that the crack existed at nanoscale and randomly distributed on the oxide shell with an average spacing at about 1–2 nm. In comparison, the phenomenon was not observed in the particle with only initial amorphous oxide shell during the same heating experiment, which further proved the formation of numerous nano-cracks in the crystallization process at ~ 400 °C.

As temperature increased to ~ 600 °C (while maintained the former oxygen pressure), the lamellas on the surface became thicker, therefore terraces were observed from the side view. Figure 4 shows the detailed process of the oxidation at ~ 600 °C, where layers of oxide nucleated at the corners of the terraces and propagated along the two surfaces. Comparable to the chemical vapor deposition (CVD)-deposition, oxide grew by single layer as well as double layers or even multi-layers, among which the single layer mode was dominant. Besides, we noticed that multiple oxide layers could nucleate simultaneously at the middle of a step (Fig. 4(a) 43 s), indicating the possibility of oxygen adsorption there. In addition, several oxide layers might grow at the same time as shown in Fig. 4(b). Once the

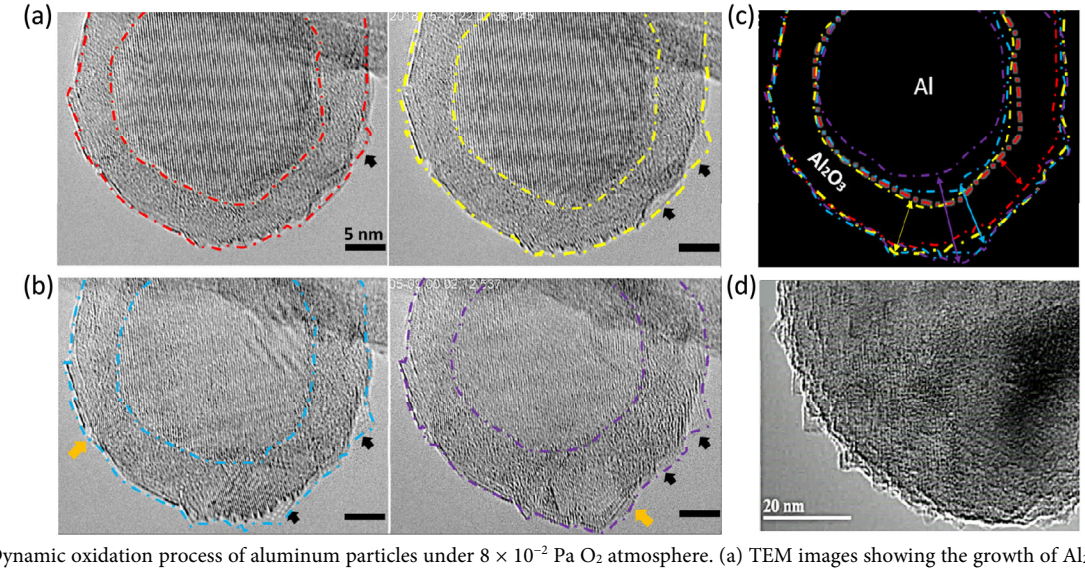

Figure 2 Dynamic oxidation process of aluminum particles under 8×10^{-2} Pa O_2 atmosphere. (a) TEM images showing the growth of Al_2O_3 lamellas at ~ 150 °C. (b) The growth of Al_2O_3 lamellas at ~ 350 °C. (c) Schematic of the evolution of interface positions of the nanoparticle in (a) and (b). (d) A HRTEM image of a particle that was heated at ~ 400 °C.

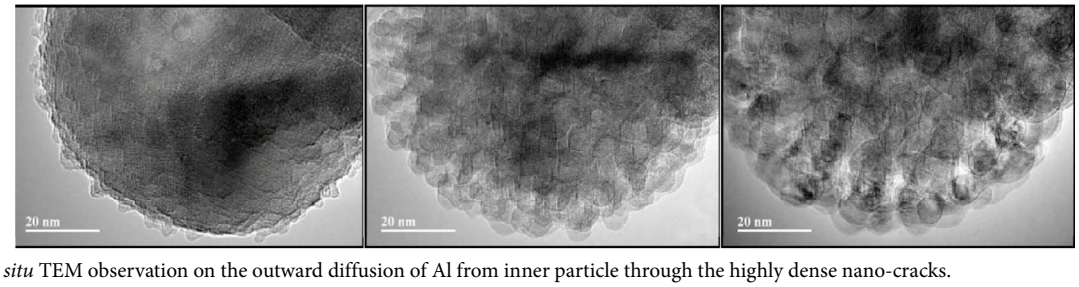

Figure 3 *In situ* TEM observation on the outward diffusion of Al from inner particle through the highly dense nano-cracks.

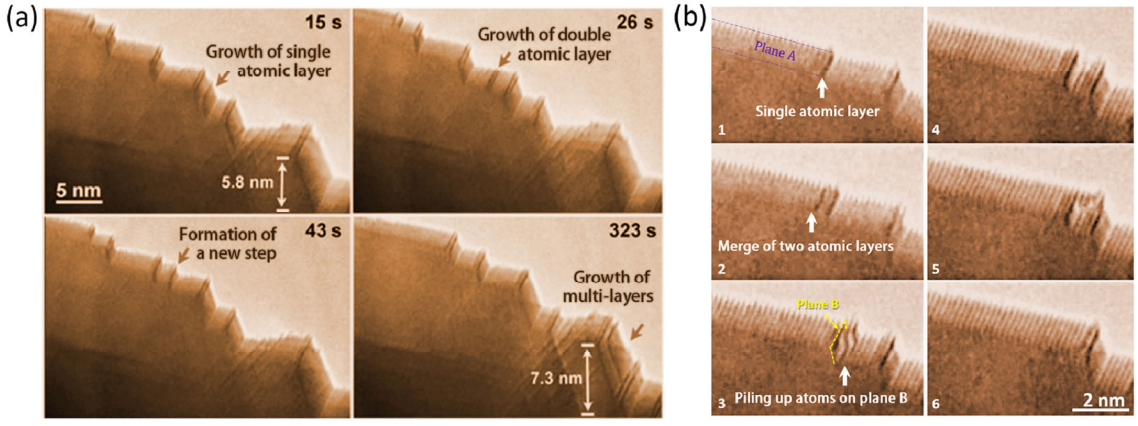

Figure 4 Time-lapsed TEM images illustrating the growth process of Al_2O_3 terraces on the surface at ~ 600 °C. (a) The multiple growth modes of oxide. (b) The merge of terraces during the growth of oxide at ~ 600 °C.

adjacent-newer oxide layer caught up with the ahead one in a faster speed along atomic plane "A", those two layers merged and gave rise to the formation of a new terrace with two surfaces of atomic plane A and a newly formed atomic plane B. Then the further reaction would like to proceed by piling up atoms, until this terrace encountered another and merged into it. And though limited by view, the oxidation reaction along atomic plane C must have happened, resulting in the thickening of the terraces.

Considering the *in situ* TEM holder was a single tilt one, post-mortem HAADF-STEM analysis was performed to characterize the atomic structure of the oxide terraces formed at ~ 600 °C. The typical atomic structure of the oxide formed at this stage is shown in Fig. 5(a). The alumina here, with a face centered cubic (FCC) structure, is similar to γ-Al_2O_3 with a spinel structure, but it owns a smaller unit cell (lattice constant about 3.95 Å) than that of γ-Al_2O_3 (lattice constant is nearly 7.90 Å). The EDX mapping results showed that the average atomic ratio of Al and O is around 37:63 (Fig. S1 and Table S1 in the ESM), a little larger than 2:3. Combining the HADDF-STEM image of Al nanoparticle (Fig. S2 in the ESM), we confirmed this structure of alumina as γ'-Al_2O_3, as defined by E. J. W. Verwey [28]. It was firstly reported that γ'-Al_2O_3 was formed by electrolytic oxidation of an aluminum electrode in boric acid solution. L. P. H. Jeurgens et al. [29] also observed this oxide phase during a oxidation process of a bare Al{111} substrates at 475 K. In this structure, each unit cell contains 4 O^{2-} in face

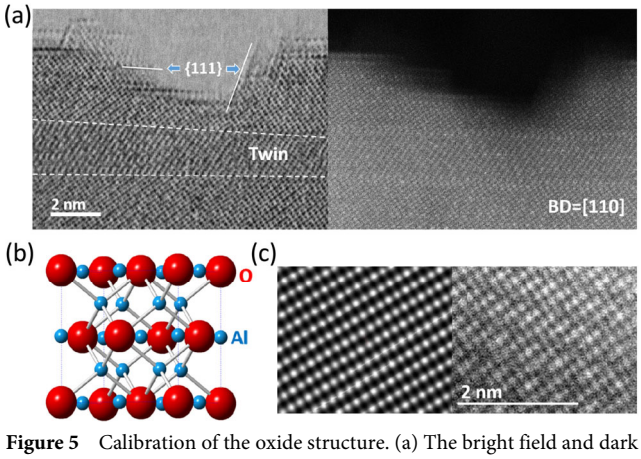

Figure 5 Calibration of the oxide structure. (a) The bright field and dark field STEM images showing the atomic structure of the oxide formed at ~ 600 °C. The crystal structure is determined to be γ'-AL_2O_3. (b) The atom model of γ'-AL_2O_3. (c) The comparison of the experimental observation of γ'-AL_2O_3 (right) with the image simulation (left).

centered positions and 8/3 Al^{3+} distributed in interstices of O^{2-}. 70% of Al^{3+} locate in octahedron hole while 30% locate in tetrahedron hole as shown in Fig. 5(b). According to the structure model of γ'-Al_2O_3, we simulated the corresponding high-resolution scanning transmission electron microscopy (HRSTEM) image in Fig. 5(c), which proved to be consistent with the HAADF image. In addition, twins were also observed in the oxide layer of γ'-Al_2O_3 with twinning plane along $(1\bar{1}\bar{1})$. It is proposed that the structure may transfer to γ-Al_2O_3 after being heated at 900 °C for a few hours and then α-Al_2O_3 if heated above 1,000 °C with the ratio of tetrahedrally-to-octahedrally coordinated Al cations decreasing [29]. Combining Fig. 5(a), we can reasonably deduce that plane A and plane B in Fig. 4(b) are $(1\bar{1}1)$ and $(1\bar{1}\bar{1})$ planes, respectively. Although plane C is invisible from this viewing direction, it presumedly belongs to {111}, which is more active for building such a structure in oxidation reaction. Given enough time, the γ'-Al_2O_3 covered the entire surface of the Al particle.

4 Conclusions

In summary, we revealed a rather complex oxidation mechanism of aluminum among a temperature range from room temperature to ~ 600 °C in a TEM. The results clearly demonstrate that the inward diffusion of oxygen contributes relatively more to the reaction at low temperatures and the outward diffusion of Al majorly controls the oxidation at high temperatures. The dynamic factors such as amorphous to crystal phase transition also influence the diffusion of Al and O. The results provide a detailed and comprehensive picture for the oxidation mechanisms of aluminum at different temperatures.

Acknowledgements

This research was supported by the Chinese 1000-Youth-Talent Plan (for Q. Y.), 111 project (No. B16042), the National Natural Science Foundation of China (No. 51671168) and the State Key Program for Basic Research in China (No. 2015CB65930).

Electronic Supplementary Material: Supplementary material (Movies ESM1–ESM4, Figs. S1 and S2, and Table S1) is available in the online version of this article at https://doi.org/10.1007/s12274-019-2593-3.

References

[1] Ermoline, A.; Dreizin, E. L. Equations for the Cabrera-Mott kinetics of oxidation for spherical nanoparticles. *Chem. Phys. Lett.* **2011**, *505*, 47–50.

[2] Jeurgens, L. P. H.; Sloof, W. G.; Tichelaar, F. D.; Mittemeijer, E. J. Growth kinetics and mechanisms of aluminum-oxide films formed by thermal oxidation of aluminum. *J. Appl. Phys.* **2002**, *92*, 1649–1656.
[3] Behler, J.; Delley, B.; Lorenz, S.; Reuter, K.; Scheffler, M. Dissociation of O_2 at Al(111): The role of spin selection rules. *Phys. Rev. Lett.* **2005**, *94*, 036104.
[4] Starodub, D.; Gustafsson, T.; Garfunkel, E. The reaction of O_2 with Al(110): A medium energy ion scattering study of nano-scale oxidation. *Surf. Sci.* **2004**, *552*, 199–214.
[5] Baran, J. D.; Grönbeck, H.; Hellman, A. Mechanism for limiting thickness of thin oxide films on aluminum. *Phys. Rev. Lett.* **2014**, *112*, 146103.
[6] Zhdanov, V. P.; Kasemo, B. Cabrera-Mott kinetics of oxidation of metal nanowires. *Appl. Phys. Lett.* **2012**, *100*, 243105.
[7] Cai, N.; Zhou, G. W.; Müller, K.; Starr, D. E. Temperature and pressure dependent Mott potentials and their influence on self-limiting oxide film growth. *Appl. Phys. Lett.* **2012**, *101*, 171605.
[8] Jones, D. E. G.; Turcotte, R.; Fouchard, R. C.; Kwok, Q. S. M.; Turcotte, A. M.; Abdel-Qader, Z. Hazard characterization of aluminum nano-powder compositions. *Propell., Explos., Pyrotech.* **2003**, *28*, 120–131.
[9] Gertsman, V. Y.; Kwok, Q. S. M. TEM investigation of nanophase aluminum powder. *Microsc. Microanal.* **2005**, *11*, 410–420.
[10] Jeurgens, L. P. H.; Sloof, W. G.; Tichelaar, F. D.; Mittemeijer, E. J. Structure and morphology of aluminium-oxide films formed by thermal oxidation of aluminium. *Thin Solid Films* **2002**, *418*, 89–101.
[11] Campbell, T.; Kalia, R. K.; Nakano, A.; Vashishta, P.; Ogata, S.; Rodgers, S. Dynamics of oxidation of aluminum nanoclusters using variable charge molecular-dynamics simulations on parallel computers. *Phys. Rev. Lett.* **1999**, *82*, 4866–4869.
[12] Sun, J.; Pantoya, M. L.; Simon, S. L. Dependence of size and size distribution on reactivity of aluminum nanoparticles in reactions with oxygen and MoO_3. *Thermochim. Acta* **2006**, *444*, 117–127.
[13] Hasani, S.; Panjepour, M.; Shamanian, M. The oxidation mechanism of pure aluminum powder particles. *Oxid. Met.* **2012**, *78*, 179–195.
[14] Zhang, S. S.; Dreizin, E. L. Reaction interface for heterogeneous oxidation of aluminum powders. *J. Phys. Chem. C* **2013**, *117*, 14025–14031.
[15] Kolarik, V.; del Mar Juez-Lorenzo, M.; Fietzek, H. Oxidation of micro-sized spherical aluminium particles. *Mater. Sci. Forum.* **2011**, *696*, 290–295.
[16] Rai, A.; Park, K.; Zhou, L.; Zachariah, M. R. Understanding the mechanism of aluminium nanoparticle oxidation. *Combust. Theor. Model.* **2006**, *10*, 843–859.
[17] Litrico, G.; Proulx, P.; Gouriet, J. B.; Rambaud, P. Controlled oxidation of aluminum nanoparticles. *Adv. Powder Technol.* **2015**, *26*, 1–7.
[18] Coulet, M. V.; Rufino, B.; Esposito, P. H.; Neisius, T.; Isnard, O.; Denoyel, R. Oxidation mechanism of aluminum nanopowders. *J. Phys. Chem. C* **2015**, *119*, 25063–25070.
[19] Park, K.; Lee, D.; Rai, A.; Mukherjee, D.; Zachariah, M. R. Size-resolved kinetic measurements of aluminum nanoparticle oxidation with single particle mass spectrometry. *J. Phys. Chem. B* **2005**, *109*, 7290–7299.
[20] Yuan, W. T.; Wang, Y.; Li, H. B.; Wu, H. L.; Zhang, Z.; Selloni A.; Sun, C. H. Real-time observation of reconstruction dynamics on TiO_2(001) surface under oxygen via an environmental transmission electron microscope. *Nano Lett.* **2016**, *16*, 132–137.
[21] Zhang, Z. J.; Fu, X. Q.; Mao, M. M.; Yu, Q.; Mao, S. X.; Li, J. X.; Zhang, Z. *In situ* observation of sublimation-enhanced magnesium oxidation at elevated temperature. *Nano Res.* **2016**, *9*, 2796–2802.
[22] Snijders, P. C.; Jeurgens, L. P. H.; Sloof, W. G. Structural ordering of ultra-thin, amorphous aluminium-oxide films. *Surf. Sci.* **2005**, *589*, 98–105.
[23] Flötotto, D.; Wang, Z. M.; Jeurgens, L. P. H.; Mittemeijer, E. J. Intrinsic stress evolution during amorphous oxide film growth on Al surfaces. *Appl. Phys. Lett.* **2014**, *104*, 091901.
[24] Trybula, M. E.; Korzhavyi, P. A. Atomistic simulations of Al(100) and Al(111) surface oxidation: Chemical and topological aspects of the oxide structure. *J. Phys. Chem. C* **2019**, *123*, 334–346.
[25] Lee, B. J.; Lee, C. S.; Lee, J. C. Stress induced crystallization of amorphous materials and mechanical properties of nanocrystalline materials: A molecular dynamics simulation study. *Acta Mater.* **2003**, *51*, 6233–6240.
[26] Jeurgens, L. P. H.; Sloof, W. G.; Tichelaar, F. D.; Mittemeijer, E. J. Composition and chemical state of the ions of aluminium-oxide films formed by thermal oxidation of aluminium. *Surf. Sci.* **2002**, *506*, 313–332.
[27] Snijders, P. C.; Jeurgens, L. P. H.; Sloof, W. G. Structure of thin aluminium-oxide films determined from valence band spectra measured using XPS. *Surf. Sci.* **2002**, *496*, 97–109.
[28] Elomari, S.; Boukhili, R.; Lloyd, D. J. Thermal expansion studies of prestrained Al_2O_3/Al metal matrix composite. *Acta Mater.* **1996**, *44*, 1873–1882.
[29] Reichel, F.; Jeurgens, L. P. H.; Richter, G. van Aken, P. A.; Mittemeijer, E. J. The origin of high-mismatch orientation relationships for ultra-thin oxide overgrowths. *Acta Mater.* **2007**, *55*, 6027–6037.